The Stability of Euclidean Wormhole Solutions

James Chryssanthacopoulos[1]

[1]University of Padova, Padova PD, Italy

`jamespeter.chryssanthacopoulos@studenti.unipd.it`

1. Introduction

In general relativity, the geometry of spacetime is a dynamic field that changes depending on the matter and energy it contains. Classical solutions to general relativity, wormholes are geometries that connect two asymptotic regions of spacetime [1]. Historically, wormhole solutions arose in the context of black holes, connecting two regions of the spacetime, but wormholes can represent more general geometries. Whatever the kind of wormhole, they are generally not humanly traversable unless supported by some exotic matter field. Although they have been studied for decades, wormholes have received renewed interest because of their role in raising and resolving issues in quantum gravity.

One aspect of quantum gravity that wormholes complicate is the AdS/CFT correspondence. A concrete example of the holographic principle, the AdS/CFT correspondence establishes a connection between a gravitational system in asymptotically anti-de Sitter space and a conformal field theory defined on its boundary [2]. Specifically, the correspondence equates the sum of all geometries in the gravitational theory to the partition function of the quantum field theory on the boundary. The sum of all geometries is captured by the path integral over all spacetime configurations. This path integral is usually taken over configurations that have a single compact boundary. The challenge arises when the gravitational theory has multiple boundaries, as in the case of wormholes. In that instance, AdS/CFT equates the gravitational theory with distinct quantum field theories over the different boundaries, but the presence of wormholes implies a correlation between these theories that is not accounted for.

A closely related issue that wormholes raise concerns the ability to factor path integrals over geometries with multiple boundaries, depicted in Figure 1. Consider the geometry with a single boundary represented by the first line. Let $\langle Z \rangle$ be the path integral over all configurations terminating in that boundary. If the geometry is duplicated, as shown on the second line, its path integral should be the product of those of the disconnected geometries, $\langle Z^2 \rangle = \langle Z \rangle^2$. The wormhole connecting the boundaries adds a contribution to the path integral that violates this factorization. In the context of AdS/CFT, this inability to factor the path integral means there are correlations between observables on the two boundaries in the gravitational theory, which implies the presence of correlations between the corresponding quantum field theories.

While wormholes challenge the traditional understanding of AdS/CFT, it is unclear the extent to which wormhole solutions contribute to the full calculation of the path integral. The path integral over all geometries is given by

$$Z = \int \mathcal{D}g \, e^{iS[g]},$$

$$\langle Z \rangle =$$

$$\langle Z^2 \rangle = \left(\qquad \qquad \right) +$$

$$\neq \langle Z \rangle^2$$

Figure 1. The path integral over all geometries with two boundaries does not factorize if a wormhole connecting the boundaries is present. This figure is adapted from [3].

where g is the metric tensor and $S[g]$ is the action functional of the theory for a given metric. Since the exponential is an oscillating function, it is common to perform a Wick rotation, introducing the Euclidean time, $t = -i\tau$. The path integral becomes

$$Z = \int \mathcal{D}g \, e^{-S[g]}.$$

Although the integral is performed over all metrics consistent with the boundary conditions, the presence of the minus sign in the exponential means that the integral is dominated by metrics that minimize the action, as shown in Figure 2. Wormholes are given by metrics that are usually found by solving the Einstein equations, but these solutions extremize the action, not necessarily minimize it. If a wormhole solution is a maximum of the action, it may not contribute significantly to the overall path integral. In that case, its role in the problems just described may be limited.
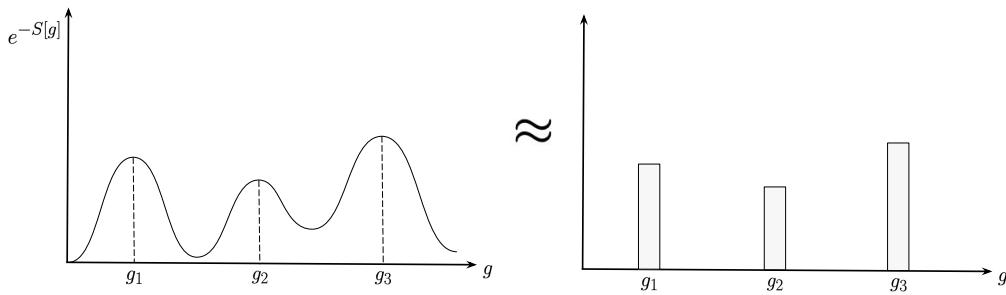

Figure 2. The gravitational path integral is the sum over all geometries, but if the configuration space is dominated by a few points with low action, the path integral can be approximated by the sum only over those metrics.

Another feature of wormholes that maximize the action is that they are unstable when perturbed. Determining whether a wormhole is unstable involves expressing the action in terms of fluctuations of the metric around the wormhole solution and checking whether it is has negative eigenvalues. These negative modes are not expected to dominate when integrated over nearby configurations in the path integral. In this way, understanding negative modes is crucial in assessing the importance of wormholes in quantum gravity.

2

One major reason why wormholes are important in quantum gravity is because they help to explain how information is recovered from a black hole. According to general relativity, anything that falls into a black hole cannot be recovered, but this conflicts with quantum mechanics, which conserves information. Combining general relativity and quantum mechanics semiclassically, it was shown that a black hole emits radiation, as shown in Figure 3. At the event horizon, one particle in a particle-antiparticle pair formed from the vacuum falls into the black hole, while the other is emitted. If the infalling particle is forever trapped inside the black hole, the entropy of the emitted radiation continuously increases. Since the AdS/CFT correspondence treats a black hole as a quantum system, information should be conserved and the entropy should eventually decrease. This evolution of entropy that increases, then decreases, is known as the Page curve. To reproduce the Page curve, wormholes are needed to compute the entanglement entropy of the radiation.
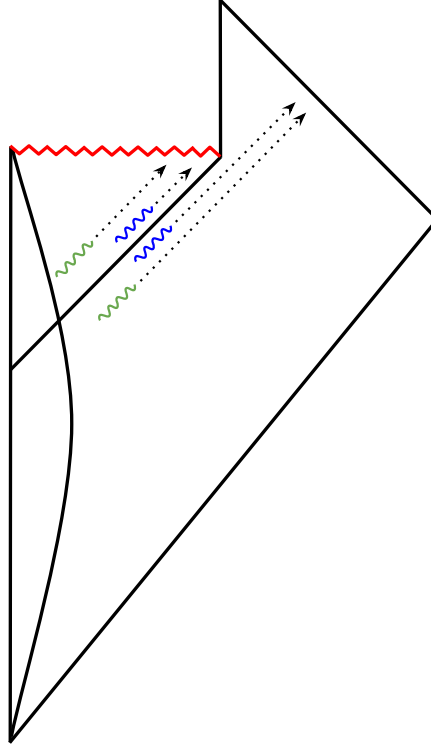

Figure 3. A black hole formed from collapsing matter emits radiation at the event horizon. One particle escapes to asymptotically Minkowski space, while the other falls into the black hole. This figure is adapted from [4].

The entropy of black hole radiation is calculated using holography. As already mentioned, holography relates a gravitational system to a quantum field theory in one fewer dimension. More concretely, there is a mapping between fields in the bulk, and gauge-invariant operators on the boundary. One example of this mapping is the duality between the bulk metric and the stress tensor on the boundary [1]. Generally, correlation functions of operators on the boundary can be computed from bulk fields. This is especially useful when the boundary theory is strongly coupled, which may correspond to a classical bulk theory with a well-known solution. Another example of the holographic mapping involves quantum information. One measure of quantum information of

a boundary region A is the von Neumann entropy

$$S_A = -\text{Tr}(\rho_A \log \rho_A),$$

where ρ_A is the reduced density matrix of the region computed by tracing over the degrees of freedom outside of A, $\rho_A = \text{Tr}_{\bar{A}}(\rho)$. On the gravitational side, the entropy can be computed using the Ryu-Takayanagi formula [5]

$$S_A = \frac{\text{Area}(\gamma_A)}{4G_N},$$

where γ_A is the codimension-two hypersurface in the bulk with minimal area that shares the same boundary as A, among other requirements. This geometry is depicted schematically in Figure 4. To account for the quantum effects of radiation in the bulk, the Ryu-Takayanagi formula needs to include an additional contribution

$$S_A = \min\left[\frac{\text{Area}(\gamma_A)}{4G_N} + S_{\text{bulk}}\right],$$

where S_{bulk} is the entanglement of the radiation induced by the presence of the surface γ_A. The minimization is carried out over all possible surfaces satisfying the constraints.
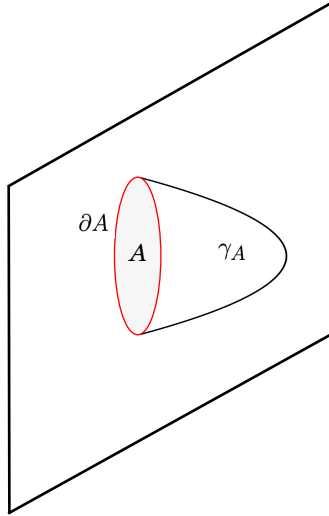

Figure 4. The entanglement entropy of quantum fields on A can be computed from the area of the codimension-two hypersurface in the bulk that shares the same boundary.

While the quantum-corrected Ryu-Takayanagi incorporates the entropy of matter fields, it is insufficient to model the entropy of radiation during black hole evaporation. That is because as the black hole shrinks, the entropy of the radiation decreases, but S_{bulk}, computed over the black hole exterior, continues to grow. To account for entanglement with radiation in the black hole interior, the entropy is given by

$$S_{\text{rad}} = \min_X\left\{\text{ext}_X\left[\frac{\text{Area}(X)}{4G_N} + S_{\text{sc}}(\Sigma_{\text{rad}} \cup \Sigma_{\text{island}})\right]\right\}, \tag{1}$$

4

where the extremization is performed over a general surface X [6]. The semiclassical entropy, S_{sc}, is computed over the union of two disconnected regions, shown in Figure 5. The region Σ_{rad} encompasses the area from a given cutoff surface to the exterior boundary, while Σ_{island} encompasses the region from the surface X to the interior boundary. As the black hole continues to evaporate, Σ_{island} grows and the semiclassical entropy decreases.
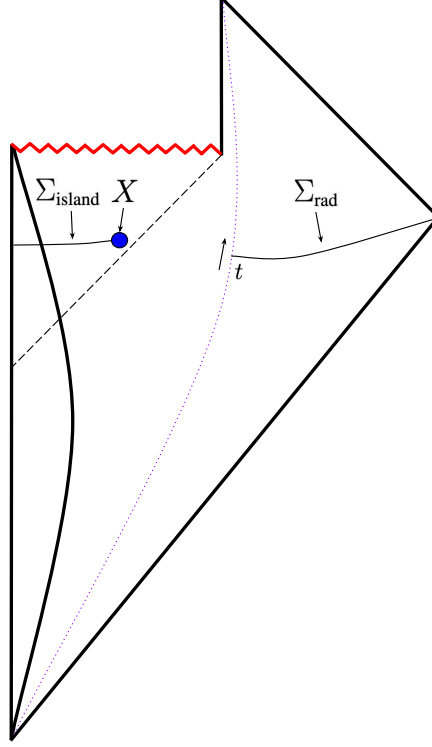

Figure 5. To compute the radiation entropy, the area of the surface X is added to the semiclassical entropy over the union between regions both outside and inside the black hole. This figure is adapted from [4].

To compute the entropy, wormholes play a crucial role. To see this, consider the initial state of radiation given by the wavefunction, $|\Psi_i\rangle$. The amplitude associated with transition to the final state, $|\Psi_f\rangle$, can be computed using the gravitational path integral

$$\langle\Psi_f|\Psi_i\rangle = \int_{g_i}^{g_f} \mathcal{D}g \, e^{-S[g]},$$

where g_i and g_f are the metrics corresponding to the geometries of the initial and final states, respectively. Because Equation 1 involves a minimum, it is natural to investigate when S_{sc} is minimized. To do so, the purity of the state can be computed, defined by $\text{Tr}(\rho^2)$. If the state is pure, meaning it has no entropy, then $\text{Tr}(\rho^2) = \text{Tr}(\rho)^2$. If the entropy is large, $\text{Tr}(\rho^2) \ll \text{Tr}(\rho)^2$. The elements of the density matrix are

$$\rho_{ab} = \langle\Psi_a|\Psi_i\rangle \langle\Psi_i|\Psi_b\rangle,$$

which is represented in Figure 6 as two black holes glued together with exterior geometries g_a and g_b. To compute $\text{Tr}(\rho^2)$, the cigar geometry is replicated and the different ways

5

of connecting them are summed over, as shown in Figure 7 [7]. In the first configuration, the geometries are disconnected. In this case, $\text{Tr}(\rho^2) \ll \text{Tr}(\rho)^2$ and the entropy is large. When the geometries are connected through a wormhole, $\text{Tr}(\rho^2) = \text{Tr}(\rho)^2$ and the entropy is zero, because the wormhole purifies the state. Note that while the introduction of wormholes generally causes the path integral not to factor, wormholes in this context actually lead to factorization of the trace. Either way, wormholes are essential in reducing the entropy during the evaporation process and reproducing the Page curve.
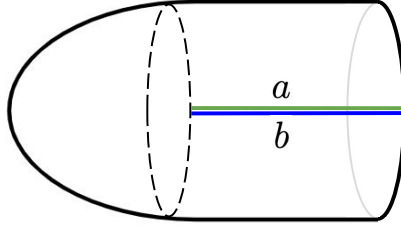

Figure 6. A schematic representation of the density matrix element ρ_{ab} of the black hole radiation. The states a and b correspond to exterior geometries that are glued together. This figure is adapted from [4].

The previous discussion highlights the importance of the path integral in calculating the entropy. As already mentioned, wormholes only contribute significantly to the path integral if they are free of negative modes. This report discusses wormhole solutions of general relativity with an eye to identifying negative modes. In Section 2, a theory with three gauge fields in four-dimensional anti-de Sitter space is considered. In Section 3, some conclusions are presented.

Figure 7. The purity is computed using replicas of the geometry that can be connected in different ways, including connecting the interiors with a wormhole. This figure is adapted from [4].

2. Einstein-Maxwell Theory with an S^3 Boundary

This section closely follows Section 4 of [3], while elaborating on the calculations and at times supplying alternative derivations. The model consists of three Maxwell fields $F^i_{\mu\nu} = \mathrm{d}A^i$ in four-dimensional AdS. The action is given by

$$S = -\int_{\mathcal{M}} d^4x \sqrt{g} \left(R + \frac{6}{L^2} - \sum_{i=1}^{3} F^i_{\mu\nu} F_i^{\mu\nu} \right) - 2\int_{\partial\mathcal{M}} d^3x \sqrt{h} K + \mathcal{S}_{\mathcal{B}}, \qquad (2)$$

6

where L is the AdS length scale, h is the determinant of the induced metric on the boundary $\partial\mathcal{M}$, and K is the extrinsic curvature associated with an outward-pointing normal to the boundary. The first integral is called the on-shell Euclidean action. The second term is the Gibbons-Hawking-York term needed to make the variational problem well-defined in the presence of a boundary. The final term, required to make the on-shell action finite, is given by

$$\mathcal{S}_{\mathcal{B}} = \int_{\partial\mathcal{M}} d^3x \sqrt{h} \left(\frac{4}{L} + L\mathcal{R} \right),$$

where $\mathcal{R}$ is the intrinsic Ricci scalar on $\partial\mathcal{M}$.

The equations of motion derived by varying Equation 2 with respect to the metric and fields are

$$R_{\mu\nu} + \frac{3}{L^2}g_{\mu\nu} = 2\sum_{i=1}^{3} \left(F^i_{\mu\rho}F^{i,\rho}_{\nu} - \frac{g_{\mu\nu}}{4}F^i_{\rho\sigma}F^{\rho\sigma}_i \right),$$
$$\nabla_\mu F^{\mu\nu}_i = 0.$$

The first equation is the trace-reversed Einstein equation, where the right-hand side is the energy-momentum of the Maxwell fields. The second equation represents the covariant Maxwell equations.

To find solutions to the equations, a spherically symmetric metric is used. The metric on the round three-sphere is

$$d\Omega^2 = \frac{1}{4}(\sigma_1^2 + \sigma_2^2 + \sigma_3^2),$$

where σ_i, expressed in terms of Euler angles, are

$$\sigma_1 = -\sin\psi\,d\theta + \cos\psi\sin\theta\,d\varphi,$$
$$\sigma_2 = \cos\psi\,d\theta + \sin\psi\sin\theta\,d\varphi,$$
$$\sigma_3 = d\psi + \cos\theta\,d\varphi,$$

with $\psi \in (0, 4\pi)$, $\theta \in (0, \pi)$, and $\varphi \in (0, 2\pi)$. The four-dimensional metric takes the form

$$ds^2 = \frac{dr^2}{f(r)} + g(r)d\Omega^2,$$

with $r \in (0, \infty)$, where $r = \infty$ corresponds to the conformal boundary. The vector potentials are given by

$$A^i = L\frac{\sigma_i}{2}\Phi(r).$$

Both disconnected and connected, or wormhole, solutions can be constructed from the metric by appropriate choice of the function g, which represents the gauge freedom of the metric.

2.1. Disconnected Solutions

To find disconnected solutions, the choice $g(r) = r^2$ is made. At $r = 0$, the round three-sphere smoothly shrinks to zero. With this choice, the metric becomes

$$g_{\mu\nu} = \begin{pmatrix} \frac{1}{f(r)} & 0 & 0 & 0 \\ 0 & \frac{1}{4}r^2 & 0 & \frac{1}{4}r^2\cos\theta \\ 0 & 0 & \frac{1}{4}r^2 & 0 \\ 0 & \frac{1}{4}r^2\cos\theta & 0 & \frac{1}{4}r^2 \end{pmatrix}.$$

The distinct Einstein equations are

$$2r^4 - L^2 r^3 f'(r) = 2L^4 \left[r^2 f(r)\Phi'(r)^2 - 4\Phi(r)^2 \right], \tag{3}$$

$$6r^4 - L^2 r^2 \left[rf'(r) + 4f(r) - 4 \right] = 2L^4 \left[4\Phi(r)^2 - r^2 f(r)\Phi'(r)^2 \right]. \tag{4}$$

The Maxwell equations reduce to

$$2r^2 f(r)\Phi''(r) + r^2 \Phi'(r)f'(r) + 2rf(r)\Phi'(r) - 8\Phi(r) = 0. \tag{5}$$

Regularity of the metric and fields requires

$$f(0) = 1,$$
$$\Phi'(r) = 0.$$

With those boundary conditions, the solutions to Equations 3–5 are

$$f(r) = 1 + \frac{r^2}{L^2},$$
$$\Phi(r) = \Phi_0 \frac{\sqrt{L^2 + r^2} - L}{\sqrt{L^2 + r^2} + L}.$$

It turns out that the energy-momentum tensor is zero, and that the disconnected solutions are vacuum solutions. The on-shell Euclidean action of the solution evaluates to

$$S_D = 8\pi^2 L^2 \left(1 + 3\Phi_0^2 \right). \tag{6}$$

2.2. Connected Solutions

Connected solutions exhibit a wormhole throat with a minimum radius r_0. To achieve this, the gauge can be set to $g(r) = r^2 + r_0^2$. There are two asymptotic regions, at $r = \pm\infty$. A global $\mathbb{Z}_2$ symmetry relates the two spheres while leaving the minimal sphere invariant.

With the new gauge choice, the unique Maxwell equation is

$$(r^2 + r_0^2)\left[2f(r)\Phi''(r) + f'(r)\Phi'(r) \right] + 2rf(r)\Phi'(r) - 8\Phi(r) = 0,$$

which simplifies to

$$\frac{d}{dr}\left[(r^2 + r_0^2)f(r)\Phi'(r)^2 - 4\Phi(r)^2 \right] = 0.$$

After integration, this becomes

$$f(r) = \frac{C + 4\Phi(r)^2}{(r^2 + r_0^2)\Phi'(r)^2}, \tag{7}$$

where C is the constant of integration. Using Equation 7, the Einstein equations are

$$2\left(r^2 + r_0^2\right)^2 - L^2\left[(r^2 + r_0^2)rf'(r) + 2r_0^2 f(r)\right] = 2CL^4,$$

$$6\left(r^2 + r_0^2\right)^2 - L^2\left[(r^2 + r_0^2)(rf'(r) + 2f(r) - 4) + 2r^2 f(r)\right] = -2CL^4.$$

Combining these two equations yields

$$\Phi'(r)^2 - \frac{L^2 r^2[C + 4\Phi(r)^2]}{(r^2 + r_0^2)\left[CL^4 + (r^2 + r_0^2)(L^2 + r^2 + r_0^2)\right]} = 0. \tag{8}$$

Rearranging, and again using Equation 7, results in

$$f(r) = \frac{CL^4 + (r^2 + r_0^2)(L^2 + r^2 + r_0^2)}{L^2 r^2}. \tag{9}$$

To avoid a singularity at $r = 0$, the integration constant must be

$$C = -\frac{L^2 r_0^2 + r_0^4}{L^4}.$$

With this choice, Equation 9 becomes

$$f(r) = \frac{L^2 + r^2 + 2r_0^2}{L^2}.$$

From Equation 8, it can be shown that the solution for Φ is

$$\Phi(r) = \Phi_* \cosh\left[\frac{2}{b}F\left(\arctan\left(\frac{r}{La}\right)\bigg|1 - \frac{a^2}{b^2}\right)\right], \tag{10}$$

where $a \equiv (1 + 16\Phi_*^2)^{1/4}$ and $b \equiv r_0/L$. The function $F(\phi|m)$ is the elliptic integral of the first kind. The elliptic integral parameters are related by

$$b = \sqrt{\frac{a^2 - 1}{2}}.$$

Figure 8 is a plot of $\Phi(r)$ for $\Phi_* = 2$ and $L = 1$. For some useful background on elliptic integrals, see Appendix A.1.

The source of the Maxwell fields corresponds to $\Phi(r)$ at $r = \infty$. Taking the $r = \infty$ limit of Equation 10, the argument of the elliptic integral becomes $\pi/2$, reducing it to the complete elliptic integral of the first kind, $K(m)$. The source Φ_0 as a function of Φ_* is then

$$\Phi_0(\Phi_*) = \Phi_* \cosh\left[\frac{2}{b}K\left(1 - \frac{a^2}{b^2}\right)\right]. \tag{11}$$
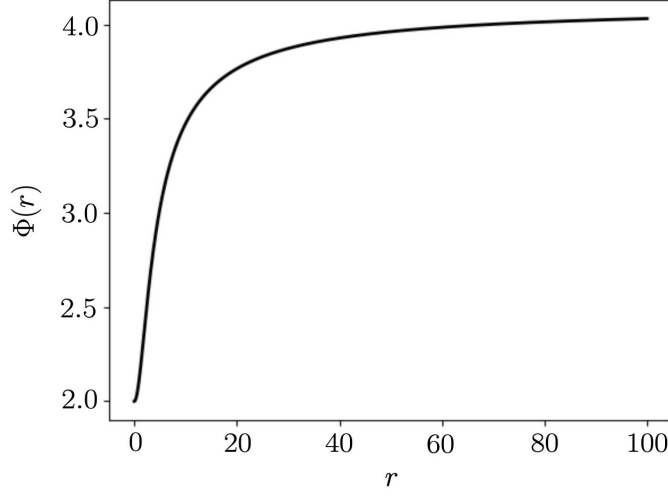
9

Figure 8. Plot of the Maxwell field solution $\Phi(r)$ involving the hyperbolic cosine of the elliptic integral of the first kind. The parameters $\Phi_* = 2$ and $L = 1$ were used.

For a single value of the source Φ_0, there can be two values of Φ_*, as shown in Figure 9. Wormhole solutions only exist if $\Phi_0 \geq \Phi_0^{\min} \approx 3.5633$, which corresponds to $\Phi_* = \Phi_*^{\min} \approx 1.0023$. The different values of Φ_* correspond to different wormhole solutions.

Another way of analyzing the two wormhole solutions is by studying how the radius of the wormhole throat changes with the source, as depicted in Figure 10. For Φ_0 above the minimum, there are two values of r_0, which correspond to small and large wormholes. At $r_0^{\min} \approx 1.2515L$, the two wormholes merge. It turns out that only the small wormhole exhibits a negative mode.

Substituting the connected wormhole solution into the on-shell Euclidean action of Equation 2, and evaluating the integral, leads to the action

$$S_C = \frac{8\pi^2 L^2}{(X-1)^{3/2}} \left[2(X-1)E(-X) - (X-2)K(-X) + \right. \tag{12}$$

$$\left. \frac{3X}{4\sqrt{X-1}} \sinh\left(4\sqrt{X-1}K(-X)\right) \right],$$

where $X \equiv 1 + L^2/r_0^2$ and $E(m)$ is the complete elliptic integral of the second kind. To assess whether the connected solution has a lower action than the disconnected one, Equation 12 can be subtracted from Equation 6 to produce the metric

$$\Delta S \equiv 2S_D - S_C,$$

which is plotted in Figure 11. The upper and lower branches correspond to the large and small wormhole, respectively. If $\Delta S > 0$, the wormhole solution has a lower action, so it should dominate in the path integral. The large wormhole is dominant for $\Phi_0 \gtrsim 3.8597$, while the small wormhole is always subdominant.

2.3. Scalar Perturbations

To identify negative modes, the metric can be perturbed around the wormhole solution. There are several types of perturbations, including scalar, vector, and tensor perturbations,
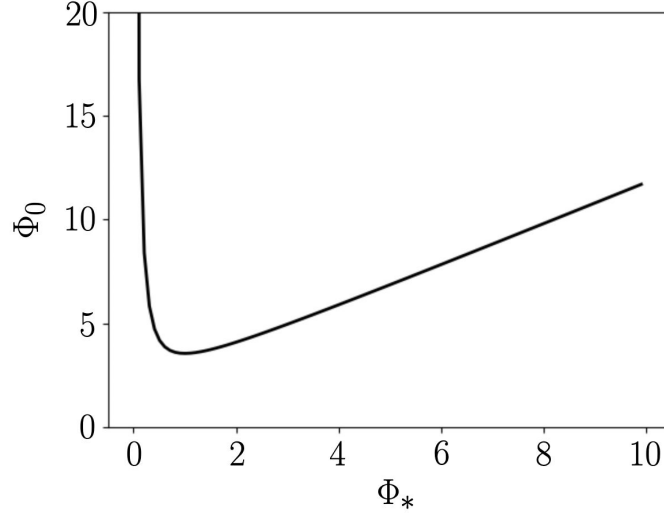
Figure 9. The source of the Maxwell fields Φ_0 as a function of Φ_*. There are two types of wormhole solutions for each value of Φ_0 above the minimum, $\Phi_0^{\min}$.

but this report will only focus on scalar perturbations. The metric and fields take the same form as before, with perturbations δg, δf, and $\delta \Phi$ applied to the background fields as

$$g(r) = \overline{g}(r) + \delta g(r),$$
$$f(r) = \overline{f}(r) + \delta f(r),$$
$$\Phi(r) = \overline{\Phi}(r) + \delta \Phi(r),$$

where $\overline{\Phi}(r)$ is given by Equation 10 and

$$\overline{g}(r) = r^2 + r_0^2,$$
$$\overline{f}(r) = \frac{L^2 + r^2 + 2r_0^2}{L^2}.$$

The action is expanded to second order in the perturbations. Integrating out the angular part, the Euclidean on-shell action is

$$S_E = \frac{\pi^2}{8L^2} \int \frac{dr}{\sqrt{fg}} \left[12L^4 \left(4\Phi^2 + fg\Phi'^2 \right) + 3L^2 \left(2fg'' + f'g' - 4 \right) - 12g^2 \right],$$

where, for simplicity, the explicit dependence on r in the various functions has been removed. The variations with respect to δg and δf

$$\frac{\delta S_E}{\delta g} = -\frac{3\pi^2}{16L^2} \int \frac{dr}{\sqrt{fg^3}} \left[12g^2 + 16L^4\Phi^2 + L^2 fg'^2 - \right.$$

$$\left. 2L^2 g \left(2fg'' + 2fL^2\Phi'^2 + f'g' - 2 \right) \right],$$

$$\frac{\delta S_E}{\delta f} = \frac{3\pi^2}{16L^2} \int \frac{dr}{\sqrt{gf^3}} \left[4g^2 - 16L^4\Phi^2 - L^2 fg'^2 + 4g \left(L^2 + L^4 f\Phi'^2 \right) \right]$$
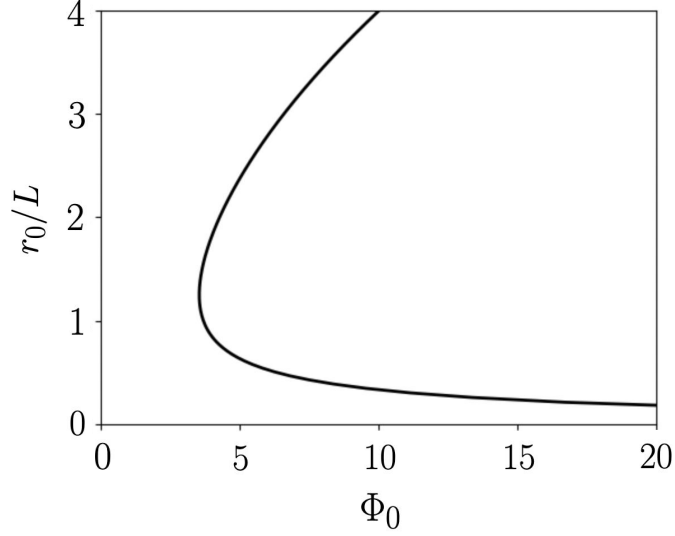
Figure 10. The radius of the wormhole throat r_0/L as a function of Φ_0. For $\Phi_0 \geq \Phi_0^{\min}$, small and large wormholes exist.

vanish because of the Einstein equations. The variation with respect to $\delta\Phi$ also vanishes because of the unique Maxwell equation

$$\frac{\delta S_E}{\delta \Phi} = -\frac{3L^2\pi^2}{2} \int \frac{dr}{\sqrt{fg}} \left(fg'\Phi' + gf'\Phi' + 2fg\Phi'' - 8\Phi \right).$$

The second-order variation of the action can be decomposed into a part dependent on δg and $\delta\Phi$ and their derivatives, and a part dependent on δf and its derivative. After integration by parts, the second part has no reliance on $\delta f'$. Using Equation 7, the f component of the second-order action is

$$S_f^{(2)} = \frac{\pi^2}{32L^2} \int \frac{dr}{(\overline{g}\overline{f})^{3/2}} \left[12L^2\overline{g}\left(L^2\overline{g}\overline{\Phi}'^2 - 3r^2 \right)\delta f^2 - 192L^4\overline{g}\overline{\Phi}\delta f\delta\Phi + \right.$$

$$48L^4\overline{f}\overline{g}^2\overline{\Phi}'\delta f\delta\Phi' + 12L^2\overline{g}\overline{f}\overline{g}'\delta f\delta g' -$$

$$\left. 3\left(16L^4\overline{\Phi}^2 + 4L^4\overline{f}\overline{g}\overline{\Phi}'^2 + L^2\overline{f}\overline{g}'^2 + 4L^2\overline{g} + 12\overline{g}^2 \right)\delta f\delta g \right].$$

This action is invariant under the infinestimal gauge transformation $\xi \equiv \xi_r(r)\partial_r$. Under this transformation, a metric perturbation h and gauge field a transform as

$$\Delta h = \mathcal{L}_\xi \overline{g},$$
$$\Delta a = \mathcal{L}_\xi \overline{A},$$

where $\mathcal{L}_\xi$ is the Lie derivative along ξ, and $(\overline{g}, \overline{A})$ are the metric and gauge potential background fields. Notice the $\overline{g}$ here is different than the $\overline{g}$ above. From the definition of
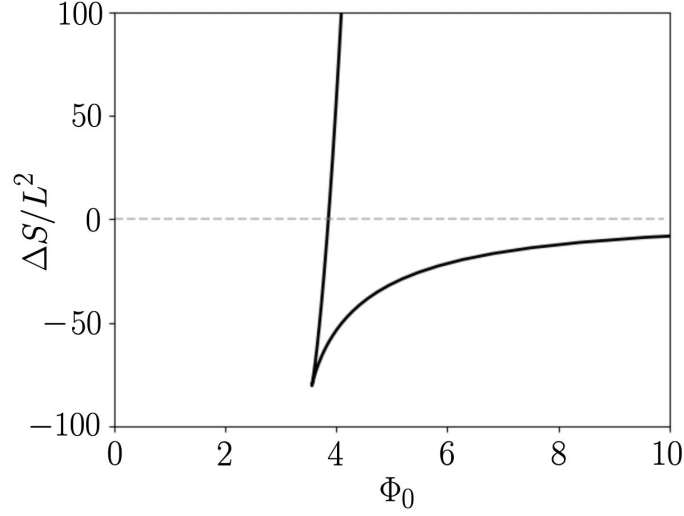
**Figure 11. The difference in the on-shell Euclidean action between the discon-
nected and connected wormhole solutions. The upper branch corresponds to
the large wormhole, which becomes dominant when $\Delta S > 0$, meaning the con-
nected solution has a lower action.**

the Lie derivative, the perturbations transform as

$$\Delta \delta f = \xi_r \overline{f}' - 2\overline{f}\xi_r', \tag{13}$$

$$\Delta \delta g = 2r\xi_r, \tag{14}$$

$$\Delta \delta \Phi = \xi_r \overline{\Phi}'. \tag{15}$$

The transformations of the perturbation derivatives are

$$\Delta \delta g' = 2\xi_r + 2r\xi_r',$$

$$\Delta \delta \Phi' = \xi_r \overline{\Phi}'' + \xi_r' \overline{\Phi}'.$$

Using these transformations, it follows that the gauge transformation of the action, $\Delta S_f^{(2)}$, is zero. Since the action is gauge invariant, it is convenient to choose $\delta g = 0$. The action simplifies to

$$S_f^{(2)} = \frac{3\pi^2}{8} \int \frac{dr}{\sqrt{\overline{f}\overline{g}^3}} \left[\left(L^2 \overline{g} \overline{\Phi}'^2 - 3r^2 \right) \delta f^2 - L^2 \overline{\Phi} \delta f \delta \Phi + 4L^2 \overline{g}^2 \overline{\Phi}' \delta f \delta \Phi' \right].$$

Given the algebraic dependence on δf in the action, the square can be completed, trans-
forming the action into the form

$$S_f^{(2)} = \int dr \left[-\left(a_1 \delta f + a_2 \delta \Phi + a_3 \delta \Phi' \right)^2 + C_0 \right],$$

where a_i are functions of the background fields only. The first term is a Gaussian integral
that can be computed, and the result can be absorbed into the measure in the path integral.

13

The remaining part involving C_0 is given by

$$S_f^{(2)} = \frac{\pi^2}{2} \int \frac{dr}{\sqrt{\overline{g}\overline{f}^3}\left(r^2 - L^2\overline{g}\overline{\Phi}'^2\right)} \left[48L^4\overline{\Phi}^2\delta\Phi^2 + 24L^4\overline{f}\overline{g}\overline{\Phi}\,\overline{\Phi}'\delta\Phi\delta\Phi' + \right.$$

$$\left. 3L^4\left(\overline{f}\overline{g}\overline{\Phi}'\right)^2\delta\Phi'^2 \right].$$

The part of the action not involving f can be expressed in terms of the gauge invariant quantity

$$q \equiv \delta\Phi - \overline{\Phi}'\frac{\delta g}{2r}.$$

Using Equations 13–15, it can be shown that $\Delta q = 0$. When $\delta g = 0$, $q = \delta\Phi$. Making that simplification, the q part of the action is

$$S_q^{(2)} = \frac{3L^2\pi^2}{2} \int \frac{dr}{\sqrt{\overline{g}\overline{f}}} \left(4q^2 + \overline{f}\overline{g}q'^2 \right).$$

The two parts of the action can be combined. After performing integration by parts on the qq' term, the result is

$$S^{(2)} = \frac{\pi^2}{4} \int dr \sqrt{\frac{\overline{g}}{\overline{f}}} \left(\overline{f}Kq'^2 + Vq^2 \right), \tag{16}$$

where

$$K \equiv \frac{6L^2r^2}{r^2 - L^2\overline{g}\overline{\Phi}'^2},$$

$$V \equiv \frac{4K}{\overline{g}} \left[\frac{2\overline{g}}{L^2r\overline{f}} \frac{L^2\left(r - L^2\overline{\Phi}\,\overline{\Phi}'\right) + \overline{g}\left(r - 2L^2\overline{\Phi}\,\overline{\Phi}'\right)}{r^2 - L^2\overline{g}\overline{\Phi}'^2} - 1 \right].$$

2.4. Negative Modes

To search for negative modes, the first term in Equation 16 needs to be integrated by parts, resulting in

$$S^{(2)} = \frac{\pi^2}{4} \int dr \sqrt{\frac{\overline{g}}{\overline{f}}}q \left[-\sqrt{\frac{\overline{f}}{\overline{g}}}\left(\sqrt{\overline{f}\,\overline{g}}Kq'\right)' + Vq \right].$$

The negative mode equation is then

$$-\sqrt{\frac{\overline{f}}{\overline{g}}}\left(\sqrt{\overline{f}\,\overline{g}}Kq'\right)' + Vq = \lambda q. \tag{17}$$

If this admits non-trivial solutions for $\lambda < 0$, the wormhole solution is locally unstable. Since $V(r)$ is symmetric around $r = 0$, modes can be decomposed into ones where

$q(0) = 0$, and others where $q'(0) = 0$. Equation 17 can be solved numerically given these boundary conditions. Since r has an infinite range, it is convenient for numerical calculations to switch to a variable with a finite range, introducing

$$r = \frac{r_0 y}{1 - y},$$

so that the conformal boundary lies at $y = 1$ and the origin at $y = 0$. Expanding the derivative in Equation 17 and changing variables, the negative mode equation becomes

$$-K\overline{f}\frac{d^2y}{dr^2}q''(y) - \left(\overline{f}\frac{dK}{dr} + \frac{rK\overline{f}}{\overline{g}} + \frac{rK}{L^2}\right)\frac{dy}{dr}q'(y) + V(r)q(y) = \lambda q(y). \qquad (18)$$

The negative mode equation can be solved numerically by discretizing it and solving the resulting matrix equation using different methods, including QZ factorization and Newton-Raphson search [8; 9]. Discretization involves choosing points on the domain, and approximating the derivatives at those points using an interpolation function. This reduces differentiation to a matrix operation

$$q'_i \approx D_{ij}q_j.$$

There are several discretization schemes that differ in their choice of grid and interpolation function. The Chebyshev method is a popular method that reduces potentially large oscillations in the interpolated function by sampling points more densely near the edges. This method was used to sample 50 points along the y axis from 0 to 0.99, which excludes the singularity at $y = 1$. See Appendix A.2 for an evaluation of the numerical accuracy.

After discretization, Equation 18 takes the form $A_{ij}q_j = \lambda B q_i$, which is the form of the generalized eigenvalue problem that can be solved using matrix factorization. To incorporate the boundary conditions, the last rows of A and B can be modified to reproduce the corresponding equations, either $q(0) = 0$ or $q'(0) = 0$. In both cases, this involves replacing the last row of B with zeros, since the boundary conditions do not involve λ. For $q(0) = 0$, the last row of A should be one at $y = 0$ and zero otherwise. For $q'(0) = 0$, the last row must be replaced by the row of D_{ij} corresponding to $y = 0$.

To determine whether the small or large wormholes exhibit negative modes, the eigenvalue problem can be solved for different values of the wormhole throat, r_0. Since $\Phi(r)$ depends on r_0 through b, adjusting r_0 results in different A matrices and different eigenvalues. Table 1 summarizes the results for the case $q'(0) = 0$. When r_0 is less than r_0^{min}, which corresponds to the small wormhole, there is one negative mode. As the wormhole becomes large, the negative mode disappears. Due to the numerical instability of the problem, these results were sensitive to the matrix entries, but the general trend of negative modes for the small wormhole, and positive modes for the large wormhole, was observed. When $q(0) = 0$, no negative modes were detected for any value of r_0.

3. Conclusion

Wormholes are important solutions to general relativity that connect two asymptotic regions of spacetime. While they have been studied for decades, they have received renewed interest because they challenge the traditional understanding of the AdS/CFT correspondence and because of their role in resolving the black hole information paradox. While

$r_0/r_0^{\mathbf{min}}$	Eigenvalues
0.8	One negative eigenvalue, $\lambda = -118$
1.0	No negative eigenvalues, $\lambda_{\min} = 1.92 \times 10^{-7}$
1.1	No negative eigenvalues, $\lambda_{\min} = 1.41 \times 10^{-6}$

Table 1. The eigenvalues of the second-order action around the wormhole solution when $q'(0) = 0$. There is one negative mode when the wormhole throat is less than $r_0^{\mathbf{min}}$, which becomes positive when $r_0^{\mathbf{min}}$ is exceeded.

many different types of wormhole solutions are possible, they only make significant contributions to the physics of a probkem if they do not contain negative modes. This report focused on examining wormhole solutions and their negative modes. Following [3], it was shown that a gravitational theory containing Maxwell fields has small and large wormhole solutions. The large wormhole solution has a lower Euclidean action than the disconnected solution when the source of the Maxwell fields exceeds a critical value. By conducting a perturbative analysis around the wormhole solution and solving the resulting eigenvalue problem numerically, it was shown that the large wormhole does not exhibit negative modes. At least for this simple model, the large wormhole solution is important and the loss of factorizability in the path integral cannot be ruled out. As [3] concluded, the factorization problem of AdS/CFT is far from resolved and will be the subject of much future research.

A. Appendix

A.1. Elliptic Integrals

Elliptic integrals historically arose in the context of finding the arc length of an ellipse [10]. They can be applied to many areas of physics, including determining the motion of a simple pendulum or the deflection of a thin elastic bar. An elliptic integral is an integral of the form

$$\int \frac{A(x) + B(x)}{C(x) + D(x)\sqrt{S(x)}}\, dx,$$

where A, B, C, and D are polynomials in x and S is a polynomial of degree three or four.

Elliptic integrals come in three different kinds. The incomplete elliptic integral of the first kind is given by

$$F(\phi|m) \equiv \int_0^\phi \frac{d\theta}{\sqrt{1 - m^2 \sin^2 \theta}}.$$

The parameter ϕ is called the amplitude, and m the modulus. The complete integral integral of the first kind is obtained by setting $\phi = \pi/2$, $K(m) \equiv F(\pi/2, m)$. The incomplete elliptic integral of the second kind is given by

$$E(\phi|m) \equiv \int_0^\phi \sqrt{1 - m^2 \sin^2 \theta}\, d\theta.$$

As before, the complete version is $E(m) \equiv E(\pi/2, m)$. The third kind is written similarly to the first two, but it is not used in this report and will not be reviewed.

A.2. Chebyshev Differentiation

To solve a differential equation numerically, the function and its derivatives need to be discretized. There are different ways of choosing discretization points and interpolating between them to approximate the derivatives. One of the simplest discretization methods is finite differencing. An example of this method is second-order central differencing, which produces the first and second derivatives at the discretization points

$$f_i' = \frac{f_{i+1} - f_{i-1}}{2\Delta x},$$
$$f_i'' = \frac{f_{i+1} - 2f_i + f_{i-1}}{\Delta x^2},$$

where Δx is the spacing between the points. Another popular method is Chebyshev differentiation. By using unevenly spaced points, it mitigates potentially large errors that occur near the edges of the domain. The discretization points are

$$x_i = \frac{1}{2}\left(x_{\min} + x_{\max}\right) + \frac{1}{2}\left(x_{\max} - x_{\min}\right)\cos\left(\frac{i\pi}{N}\right), \ i = 0, 1, \dots, N,$$

where $x_{\min}$ and $x_{\max}$ define the minimum and maximum of the domain. The differentiation matrix is given by

$$D_{ij} = \begin{cases} \sum_{k \neq i} \frac{1}{x_i - x_k}, & i = j \\ \frac{a_i}{a_j(x_i - x_j)}, & i \neq j \end{cases}$$

where

$$a_i = \prod_{j \neq i}(x_i - x_j).$$

Figure 12 shows the result of applying Chebyshev differentiation to approximate the first and second derivatives of $u(x) = e^x \sin 5x$. The blue points are the estimated derivatives at the sampled points, while the black curves are the true derivatives. When $N = 10$ points are used, the estimates track the true values, but there can be large errors. With $N = 50$ points, the reconstruction error is very small. Notice that the functions are sampled more densely near the edges.

A.3. Code

The calculations in this report were performed using Python and Mathematica. The `sympy` package in Python was used for symbolic computation, including tensor algebra. Calculations of the Ricci tensor and scalar were performed using the `einsteinpy` package. Jupyter notebooks were used to run and analyse the results. The code can be found in [11]. The relevant notebooks include

- `einstein_maxwell_ads4_euclidean`. Calculates all the quantities in the Einsten and Maxwell equations and verifies the disconnected solution
- `einstein_maxwell_ads4_euclidean_connected`. Verifies the connected wormhole solution
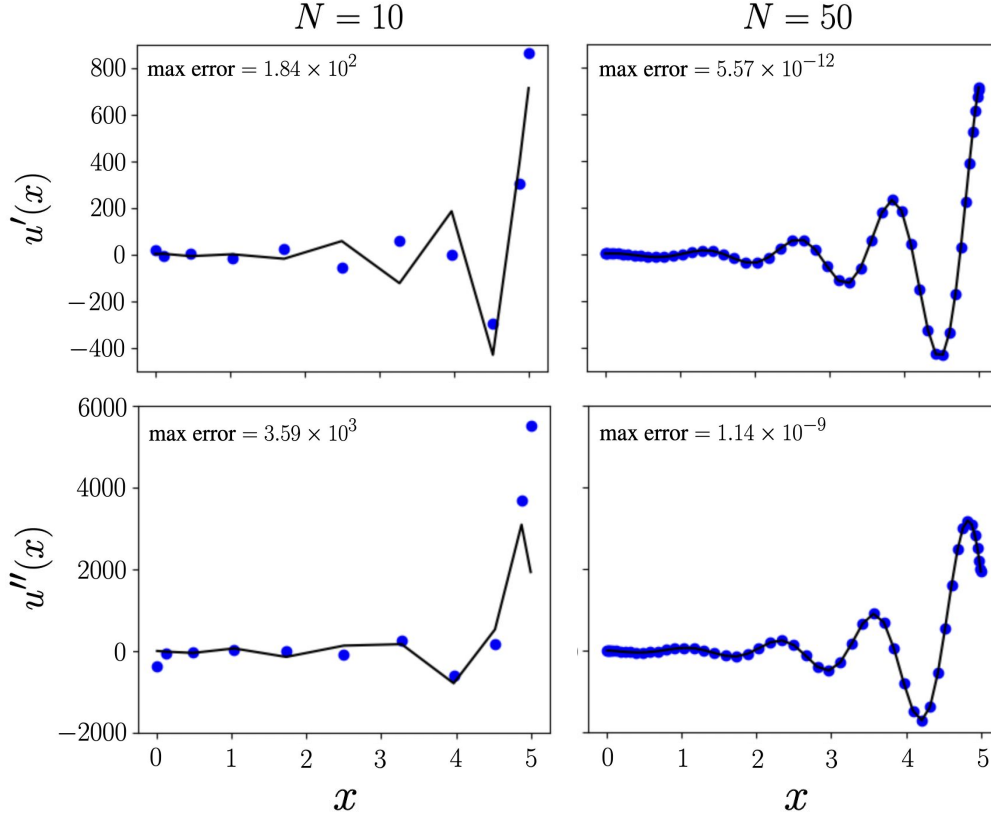- `einstein_maxwell_ads4_scalar_perturb`. Calculates the variation of the on-shell action

Figure 12. Chebyshev differentiation of $u(x) = e^x \sin 5x$ **using different amounts of discretization points. When** $N = 10$**, the estimation error of** u' **and** u'' **is large, but when** $N = 50$**, the error becomes very low.**

- `second_order_action_analysis`. Calculates the form of the second-order action
- `gauge_invariance_action`. Demonstrates the gauge invariance of the second-order action
- `negative_modes_analysis`. Demonstrates the negative modes for the small wormhole and lack of negative modes for the large wormhole

References

[1] A. Kundu, "Wormholes and Holography: An Introduction," *The European Physical Journal C*, vol. 82, no. 5, may 2022. [Online]. Available: https://doi.org/10.1140%2Fepjc%2Fs10052-022-10376-z

[2] J. Maldacena, "The Large N Limit of Superconformal Field Theories and Supergravity," *International Journal of Theoretical Physics*, vol. 38, no. 4, pp. 1113–1133, 1999. [Online]. Available: https://doi.org/10.1023%2Fa%3A1026654312961

[3] D. Marolf and J. E. Santos, "AdS Euclidean wormholes," *Classical and Quantum Gravity*, vol. 38, no. 22, p. 224002, oct 2021. [Online]. Available: https://doi.org/10.1088%2F1361-6382%2Fac2cb7

[4] A. Almheiri, T. Hartman, J. Maldacena, E. Shaghoulian, and A. Tajdini, "The Entropy of Hawking Radiation," *Reviews of Modern Physics*, vol. 93, no. 3, jul 2021. [Online]. Available: https://doi.org/10.1103%2Frevmodphys.93.035002

[5] S. Ryu and T. Takayanagi, "Holographic Derivation of Entanglement Entropy from the anti–de Sitter Space/Conformal Field Theory Correspondence," *Physical Review Letters*, vol. 96, no. 18, may 2006. [Online]. Available: https://doi.org/10.1103%2Fphysrevlett.96.181602

[6] N. Engelhardt and A. C. Wall, "Quantum Extremal Surfaces: Holographic Entanglement Entropy beyond the Classical Regime," *Journal of High Energy Physics*, vol. 2015, no. 1, jan 2015. [Online]. Available: https://doi.org/10.1007%2Fjhep01%282015%29073

[7] A. Almheiri, T. Hartman, J. Maldacena, E. Shaghoulian, and A. Tajdini, "Replica wormholes and the Entropy of Hawking Radiation," *Journal of High Energy Physics*, vol. 2020, no. 5, may 2020. [Online]. Available: https://doi.org/10.1007%2Fjhep05%282020%29013

[8] Ó. J. C. Dias, J. E. Santos, and B. Way, "Numerical Methods for Finding Stationary Gravitational Solutions," *Classical and Quantum Gravity*, vol. 33, no. 13, p. 133001, jun 2016. [Online]. Available: https://doi.org/10.1088/0264-9381/33/13/133001

[9] L. N. Trefethen, *Spectral Methods in MATLAB*. Society for Industrial and Applied Mathematics, 2000.

[10] J. R. Culham. Elliptic Integrals, Elliptic Functions and Theta functions. [Online]. Available: http://www.mhtlab.uwaterloo.ca/courses/me755/web_chap3.pdf

[11] J. Chryssathacopoulos. (2022) Analysis of Wormholes using Python. [Online]. Available: https://github.com/jchryssanthacopoulos/wormholes